PCCP

ROYAL SOCIETY OF CHEMISTRY

PAPER

View Article Online
View Journal | View Issue

Cite this: *Phys. Chem. Chem. Phys.*, 2021, **23**, 10919

Photon-induced deactivations of multiple traps in $CH_3NH_3PbI_3$ perovskite films by different photon energies

Asmida Herawati,[a] Hui-Ching Lin,[a] Shun-Hsiang Chan,[b] Ming-Chung Wu,[bc] Tsong-Shin Lim *[a] and Forest Shih-Sen Chien *[a]

Received 4th March 2021,
Accepted 23rd April 2021

DOI: 10.1039/d1cp00974e

rsc.li/pccp

Photon-induced trap deactivation is commonly observed in organometal halide perovskites. Trap deactivation is characterized by an obvious photoluminescence (PL) enhancement. In this work, the properties of traps in $CH_3NH_3PbI_3$ perovskite films were studied based on the PL enhancement excited by lasers of different wavelengths (633 nm and 405 nm). Two types of electron traps were identified; one can be deactivated by both 633 nm and 405 nm illuminations, whereas the other one can only be deactivated by 405 nm illumination. The energy levels of both types of traps were beneath the conduction band minimum. The expressions of the PL enhancement kinetics due to the trap deactivations by lasers of different wavelengths were derived. The ratio of the constants of the radiative recombination rate and the initial capture rates for both traps was determined from the PL enhancement. The trap deactivation was a photon-related process rather than a photocarrier-related process, and the deactivation time was inversely proportional to the photon flux density.

Introduction

Organometal halide perovskites (OHPs) have high optical absorption coefficients,[1,2] a wide visible absorption range,[3,4] high photoluminescence quantum yield,[5,6] efficient solar light harvesting ability,[7] and a low lasing threshold;[8,9] these are favorable properties for optoelectronic devices. After a decade of rapid developments in OHP applications, the power conversion efficiency of OHP photovoltaics has reached over 25.5% for single-junction devices[10,11] and has approached 29.1% for perovskite-based tandem devices.[11] The external quantum efficiency of OHPs as light-emitting diodes has reached 20% through management of the compositional distribution in such devices.[12] Defects in OHP material strongly limit the performance of OHP devices. In photovoltaic devices, nonradiative recombination caused by defects impair the carrier density buildup and limit the open-circuit voltage (V_{oc}). The highest V_{oc} reported for OHPs is approximately 1.18 V,[10] which is still far from the Shockley–Queisser V_{oc} limit ($\approx$1.3 eV).[13] In a light-emitting diode, the excited carrier's nonradiative recombination with defects strongly diminishes the emission of light. Deactivation or elimination of defects in OHPs is critical to improving OHP device performance. Therefore, the properties of defects in OHPs are worth exploring.

Defects can trap free charge carriers in OHPs through nonradiative recombination, and the effects of traps were quantitatively assessed through photoluminescence (PL). Many groups have studied the variation of traps in OHPs by observing PL as a function of illumination time. Tian *et al.* studied PL enhancement in OHPs by illuminating it with a laser of 514 nm wavelength in an oxygen atmosphere and proposed that the trap defects in perovskite are deactivated by photochemical reactions involving photocarriers and oxygen-related species.[14] deQuilettes *et al.* measured PL and applied time-of-flight secondary-ion-mass spectrometry when OHPs were illuminated by a 532 nm laser in conditions with a minimal amount of oxygen.[15] They found that trap state density is reduced by one order of magnitude due to the iodine's net migration. Fu *et al.* used a 532 nm laser to illuminate OHPs and found that trap deactivation is an oxygen-assisted process.[16] However, the behavior of trap deactivation is still not well studied.

In the present work, the photon-induced deactivation of traps in $CH_3NH_3PbI_3$ (methylammonium lead iodide, $MAPbI_3$) perovskite films was characterized by PL enhancement. Two lasers with wavelengths of 633 nm and 405 nm were used to excite electrons to different energy states of OHPs, and then the properties of the traps were probed. The PL enhancement

[a] *Department of Applied Physics, Tunghai University, Taichung 407224, Taiwan. E-mail: tslim@thu.edu.tw, fsschien@thu.edu.tw*
[b] *Department of Chemical and Materials Engineering, Chang Gung University, Taiyuan 33302, Taiwan*
[c] *Division of Neonatology, Department of Pediatrics, Chang Gung Memorial Hospital, Linkou, Taoyuan 33305, Taiwan*

under 633 nm and 405 nm illuminations revealed that the perovskite had two types of traps. One type can be deactivated by both 633 nm and 405 nm illuminations, whereas the other type can only be deactivated by 405 nm illumination. The expressions related to the kinetics of PL enhancement due to the trap deactivations were derived. The energy levels, initial capture rate constants, and deactivation times of the two traps were studied. The traps were deactivated directly by photons rather than by photocarriers.

Material and methods

Sample preparation

A perovskite precursor solution was prepared using methylammonium iodide (CH_3NH_3I, FrontMaterials) and lead iodide (PbI_2, 99.9985%, Alfa Aesar) in a 1.70 M indimethyl sulfoxide (DMSO, 99.9%, ECHO) and γ-butyrolactone (GBL, ≥99%, Aldrich) mixture solvent (50/50 v/v) continuously stirred at 35 °C for 12 h.[17] The perovskite precursor solution was then spin-coated onto glass slides using the solvent-engineering method.[3] Samples were stored in a vacuum-sealed plastic bag. The vacuum environment can reduce sample degradation caused by humidity and oxygen.[18–21]

Optical system

The PL measurement was performed using a modified confocal microscope (Olympus, IX71). A 633 nm laser and a 405 nm laser were used to produce illumination and PL enhancement. The laser excitation intensity was adjusted by different combinations of neutral-density filters. A bandpass filter (Chroma, 410/40 ET) was used to transmit the 405-nm laser beam and reflect the 633 nm laser beam such that the two beams could travel along the same path to the samples [Fig. 1(a)]. The laser beams were reflected by a dichroic mirror to the sample. An objective lens (Olympus, UPlanFLN 10 ×, NA = 0.3) was used to focus the beams and collect PL from the sample. The spots from the 405 nm and 633 nm lasers were monitored using an electron-multiplying CCD (Princeton instruments, Cascade 1K), and aligned to the same location on the sample, and the spot size of both lasers was the same. The sample was either illuminated by one laser or both lasers at a time. As shown in Fig. 1(b), two beam spots overlapped well with a size of about 2 μm in full width half at maximum. The PL was detected using an avalanche photodiode (MPD, PDM5CTC). The PL spectra were acquired using a monochromator (Princeton instruments, SP2150i) equipped with an electron-multiplying CCD.

Results and discussion

Fig. 2(a) shows the absorption spectrum of the $MAPbI_3$ perovskite sample. The spectrum is consistent with those found in other studies.[7,22,23] The broad absorption spectrum of perovskites is correlated with several transition levels of electrons. The absorption peaks located at 730 nm and 495 nm correspond to the 1.6 eV bandgap transition at the *R* point of the Brillouin zone of the

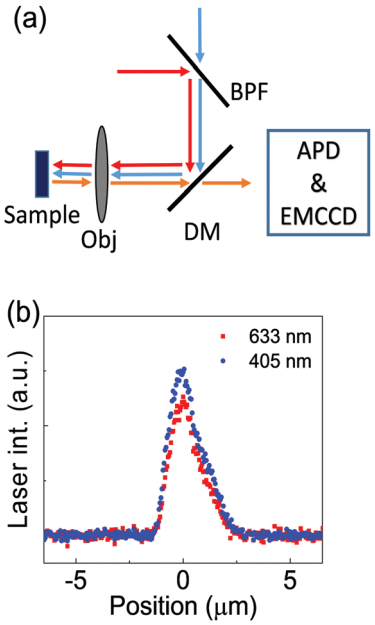

Fig. 1 (a) Experimental scheme of PL measurement. BPF: Bandpass filter. DM: dichroic mirror. Obj: objective. APD: avalanche photodiode. EMCCD: electron-multiplying CCD. Blue, red, and orange arrows denote the 405 nm laser light, 633 nm laser light, and PL, respectively. (b) Spot profiles of the 633 nm and 405 nm lasers.

*Pm*3*m* space group from the valence band maximum (VBM) to the conduction band minimum (CBM) and the 2.5 eV band-to-band transition at the *M* point to a higher conduction band (CB), respectively.[22,24] The red and blue dash arrows in Fig. 2(a) indicate the positions of the excitation wavelengths, 633 nm and 405 nm, used in this work. The 633 nm laser excited the band-to-band transition located between *R* and *M* points, and the 405 nm excited the transition located between *M* and *X* points. Both of the PL spectra excited by the 633 nm and 405 nm lasers have the same shape and a peak at 778 nm [Fig. 2(a)]. The photo-excited electrons to a higher level at the CB relax to CBM at the *R* point and recombine with the holes at the VBM to emit photons at 778 nm. The wavelength of the PL peaks does not change with an increase in illumination time. Therefore, the variation in PL intensity with illumination time observed in this work was not caused by thermal effects[16] or phase changes.

As observed in numerous other works, the intensity of the PL spectra had an obvious increase when the perovskite films were continuously illuminated by the excitation lasers. Fig. 2(b) displays the representative results of the PL intensity as a function of the time that the films were excited by the two lasers at different locations. The PL enhancement is characterized by a fast-process region and a slow-process region. The fast process is attributed to the trap filling or other processes which is not the focus of this research. The trap filling process refers to the dynamic process whereby defects repeatedly trap and release carriers and finally reach equilibrium when trapping and de-trapping rates balance.[16] The process causes a rapid initial PL increase during the first 5–10 μs of exposure before saturation.[25] The slow process is attributed to trap deactivation.

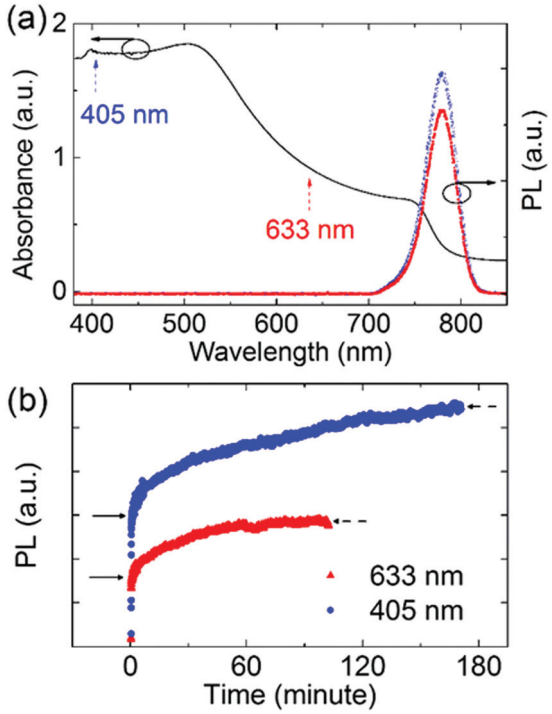

Fig. 2 (a) Absorbance (black solid curve) and PL (red solid squares for the 633 nm excitation and blue empty squares for the 405 nm excitation) spectra of $MAPbI_3$ perovskite films. (b) PL intensity as a function of the illumination time excited by the 633 nm laser with an intensity of 0.9 W cm^{-2} and the 405 nm laser with an intensity of 1.1 W cm^{-2}. The solid arrows indicate the onset of the slow PL enhancement, and the dash arrows indicate the saturated PL.

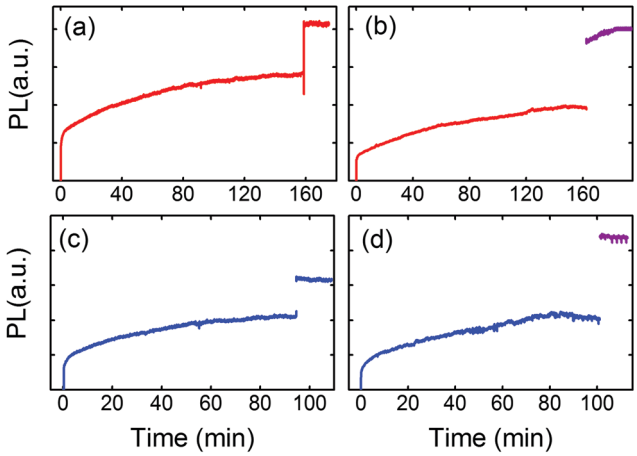

Fig. 3 PL intensity as a function of the illumination time with specific sequences of lasers applied. (a) (in red) 633 nm laser with an intensity of 11.2 W cm^{-2} was first applied and then the intensity was increased to 16.2 W cm^{-2}. (b) (in red) 633 nm laser with an intensity of 8.4 cm^{-2} was first applied, and then (in purple) 405 nm laser with an intensity of 8.9 cm^{-2} was added. (c) (in blue) 405 nm laser with an intensity of 8.9 W cm^{-2} was first applied, and then the intensity was increased to 12.9 W cm^{-2}. (d) (in blue) 405 nm laser with an intensity of 8.9 W cm^{-2} was first applied, and then (in purple) 633 nm laser with an intensity of 8.4 W cm^{-2} was added.

In this study, we solely focused on the slow trap deactivation process. The end of the fast enhancement is taken as the onset of the slow process. The initial PL intensity of the slow process I_0 is indicated by solid arrows, and the saturated PL intensity I_∞ is indicated by dash arrows. The PL intensity is proportional to $k_r/(k_r + k_{nr} + k_T)$, where k_r is the radiative recombination rate constant of free electrons and holes, k_T is the rate constant of free electrons captured by traps that can be deactivated by light illumination, and k_{nr} is the recombination rate constant by other nonradiative transitions. k_T depends on the properties and the density of traps, and decreases with illumination time due to trap deactivation. When PL saturates, k_T equals zero. We defined a trapping ratio $R_T = (I_\infty - I_0)/I_\infty$, which is equal to $k_{T0}/(k_r + k_{nr} + k_{T0})$. Here, k_{T0} is the initial value of k_T. Therefore, the capture rate of photoelectrons by the traps before the trap deactivation was proportional to R_T. R_T can act as an index of the initial quality of the $MAPbI_3$, meaning that the lower the R_T value is, the less the amount of photoelectrons are captured. As shown in Fig. 2(b), R_Ts for 633 nm and 405 nm illuminations (R_{T633} and R_{T405}) were 0.39 and 0.61, respectively. These are lower than the R_T values reported in other studies, which range from 0.83 to 0.9.[14–16] Furthermore, the substantial difference between R_{T633} and R_{T405} indicates that at least two types of traps might have been deactivated by the illumination.

To explore the different trap types, the lasers were applied to the sample at the same location in specific sequences. One laser was first used to deactivate the traps related to the laser until the end of the first slow PL enhancement, and then the other laser was added to illuminate the sample. If the traps could be deactivated by either laser, all traps would be deactivated by the first laser and no second slow PL enhancement would appear when the other laser is added. By contrast, if different types of traps were deactivated by different lasers, a second slow PL enhancement would appear when the other laser was added, after the first slow PL enhancement with the first laser. Since deactivation of traps usually needs a long time of illumination (from some hundred seconds to some hours), a higher laser intensity density up to 19 W cm^{-2} was used to excite the samples to accelerate the deactivation process in this work. According to ref. 26 excitation intensity below 100 W cm^{-2} is in low-excitation region. Fig. 3(a) presents the PL intensity as a function of time when the sample was first illuminated by a 633 nm laser with an intensity of 11.2 W cm^{-2} and then increased to 16.2 W cm^{-2}. The PL intensity exhibited a first slow enhancement and then saturated. As the laser intensity was increased, only a steep increase was observed without a second slow enhancement. The result indicates that all traps related to the 633 nm illumination were completely deactivated when the PL intensity saturated. In Fig. 3(b) the PL intensity is plotted as a function of time when the 633 nm laser with an intensity of 8.4 W cm^{-2} was first applied and then the 405 nm laser with an intensity of 8.9 W cm^{-2} was added. After the saturation of the first slow PL enhancement with the 633 nm laser, a second slow PL enhancement appeared with the addition of the 405 nm laser. The second slow PL enhancement indicated that perovskite films contain two types of traps. The first type of trap (T_1) was deactivated by a 633 nm illumination and the second type of trap (T_2) was deactivated by a 405 nm illumination.

Fig. 3(c) shows PL intensity as a function of time, where the sample was first illuminated by the 405 nm laser with an intensity of 8.9 W cm^{-2} and then increased to 12.9 W cm^{-2}. After the first PL enhancement saturated, the T_2 traps were completely deactivated; no second slow enhancement was observed as the laser intensity was increased. Similarly, the sample was illuminated first by the 405 nm laser with an intensity of 8.9 W cm^{-2} and then the 633 nm laser with an intensity of 8.4 W cm^{-2} was added, as illustrated in Fig. 3(d). No second slow PL enhancement was observed with the addition of the 633 nm laser, which means that T_1 had also been deactivated by the 405 nm laser. The result indicates that both T_1 and T_2 were deactivated by the 405 nm illumination. Therefore, T_1 can be deactivated by both the 633 nm and 405 nm illuminations, whereas T_2 can only be deactivated by illumination with the 405 nm laser. From the results, the rate equations of the deactivations of T_1 and T_2 are given as

$$\frac{dN_1}{dt} = -D_{1r}N_1 - D_{1b}N_1, \quad (1)$$

and

$$\frac{dN_2}{dt} = -D_{2b}N_2, \quad (2)$$

where N_1 and N_2 are the concentrations of T_1 and T_2, respectively. D_{1b} and D_{1r} represent the deactivation coefficients of T_1 induced by the 405 nm and 633 nm illuminations, respectively, and D_{2b} represents the deactivation coefficient of T_2 induced by the 405 nm illumination. Deactivation coefficients were suggested to be the functions of either photon density or photocarrier density, depending on the proposed mechanism.[14,15,27] The decay of N_i is obtained as follows:

$$N_1 = N_{10}\exp(-t/\tau_1), N_2 = N_{20}\exp(-t/\tau_1), \quad (3)$$

where N_{i0}, with i =1, 2, is the initial density of T_i, $\tau_1 = 1/(D_{1r} + D_{1b})$ is the deactivation time of T_1, and $\tau_2 = 1/D_{2b}$ is the deactivation time of T_2. τ_i is useful to explore the properties of trap deactivation.

The energy level of T_2 is crucial to the relaxation of the photoelectrons excited by the 405 nm laser and the behavior of T_2 deactivation. The energy level of T_2 can be obtained by the application of the two lasers in the following sequence. Firstly the 633 nm illumination is applied to deactivate all T_1, secondly the 405 nm illumination is applied to deactivate all T_2, and thirdly the 633 nm illumination is applied again. If the energy level of T_2 is higher than the CBM the photoelectrons excited to CB by the 633 nm laser are not trapped by T_2. Thus, after T_2 is deactivated in the second step (illumination with the 405 nm laser) the PL intensity excited by the 633 nm illumination in the third step should be the same before and after the second step of 405 nm illumination. If the energy level of T_2 is below the CBM, the photoelectrons excited by 633 nm will be trapped by T_2 too. The deactivation of T_2 results in the increase of the photoelectron density in CB excited by the 633 nm illumination. Therefore, the PL intensity excited by the 633 nm laser should increase after T_2 is deactivated by the 405 nm illumination. In that scenario, the sample was illuminated by the 633 nm laser with an intensity of 17 W cm^{-2}, then by the 405 nm laser with an intensity of 19 W cm^{-2}, and finally by the 633 nm laser with an intensity of 17 W cm^{-2} [Fig. 4(a)]. After T_2 was deactivated by the 405 nm laser in the second step, the PL intensity excited by the 633 nm laser was enhanced. The result indicates that the energy level of T_2 was beneath the CBM. In addition, T_2 was not deactivated as T_2 was filled with photoelectrons excited by 633 nm laser but was deactivated only by 405 nm illumination. This suggested that T_2 was deactivated by the 405 nm photons rather than by the photocarriers.

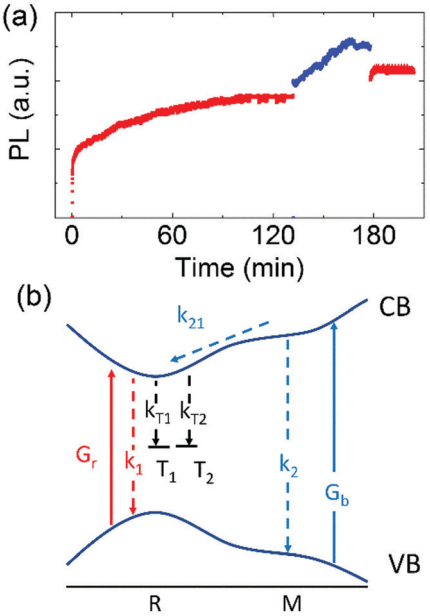

Fig. 4 (a) PL intensity as a function of laser illumination time. The sample was first excited by the 633 nm laser with an intensity of 17 W cm^{-2} (in red), then by the 405 nm laser with an intensity of 19 W cm^{-2} (in blue) and finally 633 nm with an intensity of 17 W cm^{-2} (in red). (b) Schematic of the energy diagram of $CH_3NH_3PbI_3$ and the electron transitions.

The experimental results were summarized into a scheme of electron transitions, including the electrons captured by T_1 and T_2, as shown in Fig. 4(b). This scheme involves only electron trapping without hole trapping, because electron traps have been identified as the dominant source of trap-assisted recombination in $CH_3NH_3PbI_3$.[28] G_b and G_r are electron generation rates by 405 nm and 633 nm illuminations, respectively. k_{21} is the electron relaxation rate constant from M point to R point and k_2 is the recombination rate constant for other nonradiative transitions from M point. Electrons in the CBM either relax to the valence band or are captured by the traps. k_1 includes radiative and nonradiative processes (k_r and k_{nr}, respectively). k_{Ti}, where i = 1,2, denotes the capture rate constant of electrons by T_i and is expressed as $k_{Ti} = C_iN_i(1 - f_i)$, where f_i is the filling fraction of T_i, and C_i is the capture coefficient of T_i. Exciton formation, dissociation, and decay were considerably fast processes compared with the deactivation process. Therefore, these exciton-related processes were considered in the thermal equilibrium, and the contribution of excitons to the variation of

electron density was ignored.[25] The trapping process, which is much faster than the deactivation process, is considered as being in equilibrium and was ignored in our scheme, and f_i is assumed to be a constant during the deactivation as the trapping process is in equilibrium. On the basis of the scheme, the trapping ratio with the 633 nm illumination is given as

$$R_{T633} = \frac{k_{T10}}{k_1 + k_{T10} + k_{T20}}, \quad (4)$$

which is the ratio of photocarriers captured by T_1. The ratio with 405 nm illumination is given as

$$R_{T405} = \frac{k_{T10} + k_{T20}}{k_1 + k_{T10} + k_{T20}}, \quad (5)$$

which is the ratio of photocarriers captured by both T_1 and T_2, and k_{Ti0}, i = 1, 2, is the initial value of k_{Ti}. R_{T405} is larger than R_{T633}, which is consistent with our experimental results displayed in Fig. 2(b).

To explore the trapping ratios and deactivation times, the PL enhancement under various excitation intensities (0.4–11.2 W cm^{-2} for 633 nm laser and 0.6–7.7 W cm^{-2} for 405 nm) were measured, as depicted in Fig. 5(a) and (b). R_{T633} and R_{T405} were obtained under different excitation intensities [Fig. 5(c)]. Both ratios are power independent (average values are 0.34 and 0.51), which indicates that f_i is a constant within the range of the excitation intensity. The ratio of k_1, k_{T10}, and k_{T20} was 0.49 : 0.35 : 0.16 for our samples. The sum of the ratios of photon carriers captured by the traps (0.35 and 0.16) before deactivation was 0.51, which is rather high in terms of solar power harvesting and light emission applications.

The deactivation time from the PL enhancement can be derived from the rate equations for electron densities,

$$\frac{dn'}{dt} = G_b - n'(k_{21} + k_2), \quad (6)$$

$$\frac{dn}{dt} = G_r + n'k_{21} - n(k_1 + k_{T1} + k_{T2}), \quad (7)$$

which are similar to those in ref. 16, and n' and n represent the electron densities in M point and in R point, respectively. Because the deactivation processes occurred in a time scale of seconds to minutes, n' and n had reached their quasi-equilibrium states. Combining N_i from eqn (3), (6) and (7), gives n_r and n_b, the electron densities with respect to the 633 nm and 405 nm illuminations, which are expressed as follows:

$$n_r = \frac{G_r}{k_1 + k_{T10}\exp(-t/\tau_{1r}) + k_{T20}} \quad (8)$$

$$n_b = \frac{\frac{G_b k_{21}}{k_{21} + k_2}}{k_1 + k_{T10}\exp(-t/\tau_{1b}) + k_{T20}\exp(-t/\tau_{1b})} \quad (9)$$

where $\tau_{1b} = 1/D_{1b}$ and τ_{2b} are the τ_1 and τ_2 under the 405 nm illumination, respectively, and τ_{1r} (= $1/D_{1r}$) is τ_1 under the 633 nm illumination. In the presence of traps, the PL intensity

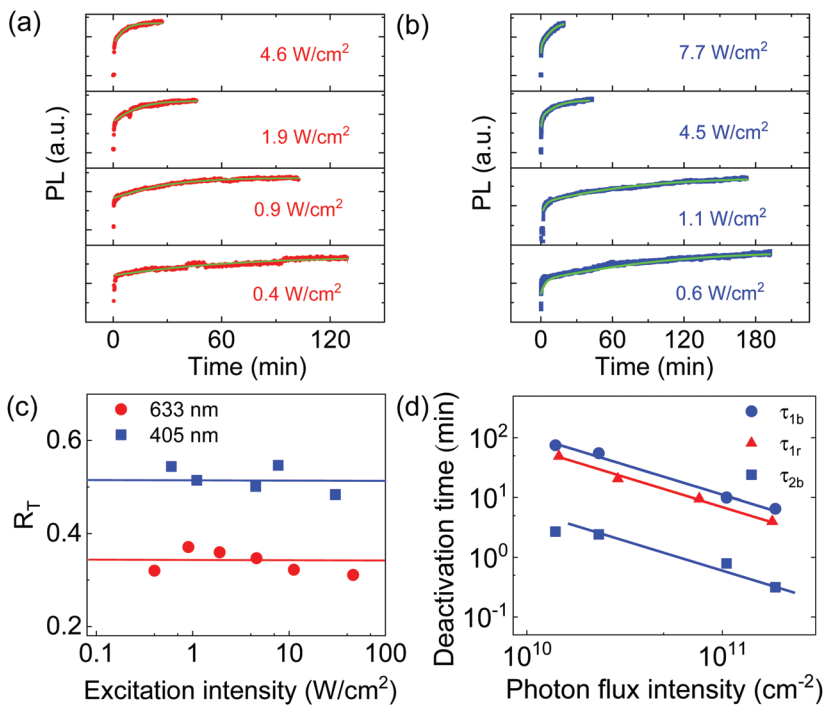

Fig. 5 PL intensity as a function of illumination time excited by (a) 633 nm and (b) 405 nm lasers with different excitation intensities. The green curves in (a and b) are fitted results with eqn (8) and (9), respectively. (c) R_T for different excitation intensities of the 633 nm and 405 nm lasers. Solid lines represent average values of 0.34 and 0.51. (d) The deactivation time derived for each type of trap fitted to the data in (a and b) as a function of the photon flux intensity. Solid lines with a slop of −1 are used as guiding lines of sight.

is proportional to n at low-excitation rate,[25] so we can use n as a function of time to represent the kinetics of the PL intensity.

The saturation time decreased as the photon density increased, as illustrated in Fig. 5(a) and (b). The kinetics of the PL enhancements in Fig. 5(a) and (b) were well fitted to eqn (8) and (9), respectively, where τ_{1b}, τ_{1r}, and τ_{2b} (as well as D_{1b}, D_{1r} and D_{2b}) were considered as fixed values for each photon density. Fig. 5(d) shows the fitted τ_{1b}, τ_{2b}, and τ_{1r} under various photon flux intensities. Those two deactivation times related to 405 nm differ by two order of magnitude. If the underlying mechanisms of the deactivation of T_1 by 633 nm light and 405 nm light are the same, τ_{1r} and τ_{1b} should be close to each other. Therefore, the one closer to τ_{1r} was designated as τ_{1b}. τ_{2b} is two order of magnitude smaller than τ_{1b}, indicating that T_2 was much more reactive than T_1 to the 405 nm illumination. We suggest that the radical states of T_2 are much more reactive than those of T_1.

As observed in the experimental results of the present experiment, τ_{1b}, τ_{1r}, and τ_{2b} were inversely proportional to the excitation intensity (P), *i.e.*, $\tau \times P$ = constant. In our case, $\tau \times P = 10^{12}$ min s^{-1} cm^{-2} (or 50 min W cm^{-2} for 405 nm) according to the results in Fig. 5(d). An optical pretreatment to deactivate the traps in $MAPbI_3$ films can improve the performance of $MAPbI_3$ solar cells.[29] Under proper "dosage" of illumination, the performance of $MAPbI_3$ in optoelectronics should be optimized in terms of trap deactivation. The proper dosage is exactly $\tau \times P$.

It has been proposed that such traps are deactivated by the trapped photocarriers and oxygen-related species, implying that the deactivation times as well as the deactivation coefficients are functions of electron density.[14] The kinetics of PL enhancement, which are well described by eqn (8) and (9), illustrates the increase of electron density with illumination time, which means the deactivation time should decrease with illumination time. However, the kinetics of the PL enhancements were well fitted by eqn (8) and (9) with fixed values of deactivation times. Therefore, the deactivation time is a function of excitation intensity, but not a function of photocarrier density. We suggest that the deactivations of T_1 and T_2 by illumination using the 633 nm laser, the 405 nm laser, or both lasers are a photon-activated process rather than an electron-activated process.

Research by deQiulettes *et al.* suggests that illumination induces the migration and redistribution of iodine,[15] resulting in PL enhancement with net reduced trap densities, and that oxygen may not be essential in the process. Anaya *et al.* proposed that the annihilation of halide vacancy and interstitial Frenkel pairs[30] is favored when the surface density of O_2^- that forms on the sample surface induced by photoexcitation of adsorbed oxygen is sufficiently high to activate the migration of interstitial halide anions away from the surface and toward the bulk.[27] The density of traps in the bulk of the material is then reduced, and the reinforcement of PL is observed. Here, the formation of adsorbed O_2^- on the surface upon illumination is crucial for the deactivation and reduction of traps. In both cases, the deactivation (or reduction) of traps depends on the illumination photon density rather than photocarrier density, which is in agreement with our argument explaining the process of trap deactivation. However, these two studies are controversial about the role of oxygen in the deactivation process. To examine the effects of environmental conditions on the deactivation, PL was measured with perovskite samples placed in vacuum-sealed plastic bags and in air excited by both 633 nm and 405 nm. As shown in Fig. 6(a) and (b), deactivation times are obviously shorter when samples were exposed to air by both wavelengths. This result suggests that oxygen plays a key role in the mechanism of deactivation.

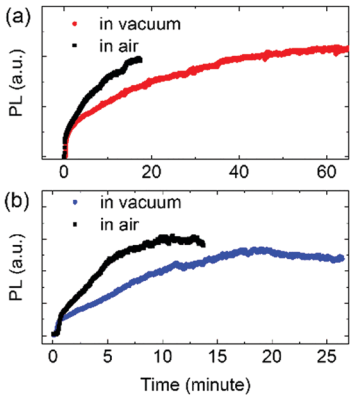

Fig. 6 PL intensity as a function of the illumination time with samples placed in vacuum-sealed plastic bags and in air illuminated by (a) 633 nm laser and (b) 405 nm laser.

Conclusions

We studied photon-induced trap deactivation in $MAPbI_3$ perovskite films by analyzing PL enhancement of perovskite samples excited by 633 nm and 405 nm lasers. Two types of traps (T_1 and T_2) were identified in perovskite films. T_1 was deactivated by both 633 nm and 405 nm illuminations, whereas T_2 was deactivated only by 405 nm illumination. The energy levels of T_1 and T_2 were both beneath the CBM. The expressions of the PL enhancement kinetics related to the trap deactivation under the 633 nm and 405 nm illuminations were derived. The ratio of the constants of the radiative recombination rate and the initial capture rate by T_1 and T_2 can be determined from the PL enhancement. The kinetics of the PL enhancement indicated that the deactivation time was inversely proportional to the photon flux density and the traps were directly deactivated by illuminating photons rather than by photocarriers.

Conflicts of interest

There are no conflicts to declare.

Acknowledgements

This work was supported by the Ministry of Science and Technology, Taiwan (MOST 109-2112-M-029-001 & 109-2112-M-029-006).

References

1 N. Pellet, P. Gao, G. Gregori, T.-Y. Yang, M. K. Nazeeruddin, J. Maier and M. Grätzel, *Angew. Chem., Int. Ed.*, 2014, **53**, 3151–3157.
2 Y. Zhao, A. M. Nardes and K. Zhu, *Faraday Discuss.*, 2014, **176**, 301–312.
3 N. J. Jeon, J. H. Noh, Y. C. Kim, W. S. Yang, S. Ryu and S. I. Seok, *Nat. Mater.*, 2014, **13**, 897–903.
4 S. D. Stranks, G. E. Eperon, G. Grancini, C. Menelaou, M. J. P. Alcocer, T. Leijtens, L. M. Herz, A. Petrozza and H. J. Snaith, *Science*, 2013, **342**, 341–344.
5 S. D. Stranks, R. L. Z. Hoye, D. Di, R. H. Friend and F. Deschler, *Adv. Mater.*, 2019, **31**, 1803336.
6 S. D. Stranks and H. J. Snaith, *Nat. Nanotechnol.*, 2015, **10**, 391–402.
7 S. De Wolf, J. Holovsky, S.-J. Moon, P. Löper, B. Niesen, M. Ledinsky, F.-J. Haug, J.-H. Yum and C. Ballif, *J. Phys. Chem. Lett.*, 2014, **5**, 1035–1039.
8 Z. Duan, S. Wang, N. Yi, Z. Gu, Y. Gao, Q. Song and S. Xiao, *ACS Appl. Mater. Interfaces*, 2017, **9**, 20711–20718.
9 H. Zhu, Y. Fu, F. Meng, X. Wu, Z. Gong, Q. Ding, M. V. Gustafsson, M. T. Trinh, S. Jin and X. Y. Zhu, *Nat. Mater.*, 2015, **14**, 636–642.
10 M. Jeong, I. W. Choi, E. M. Go, Y. Cho, M. Kim, B. Lee, S. Jeong, Y. Jo, H. W. Choi, J. Lee, J.-H. Bae, S. K. Kwak, D. S. Kim and C. Yang, *Science*, 2020, **369**, 1615–1620.
11 National Renewable Energy Laboratory. Best research-cell efficiencies chart 2020, www.nrel.gov/pv/assets/pdfs/best-research-cell-efficiencies.20200925.pdf (accessed January 2021).
12 K. Lin, J. Xing, L. N. Quan, F. P. G. de Arquer, X. Gong, J. Lu, L. Xie, W. Zhao, D. Zhang, C. Yan, W. Li, X. Liu, Y. Lu, J. Kirman, E. H. Sargent, Q. Xiong and Z. Wei, *Nature*, 2018, **562**, 245–248.
13 W. E. I. Sha, X. Ren, L. Chen and W. C. H. Choy, *Appl. Phys. Lett.*, 2015, **106**, 221104.
14 Y. Tian, M. Peter, E. Unger, M. Abdellah, K. Zheng, T. Pullerits, A. Yartsev, V. Sundström and I. G. Scheblykin, *Phys. Chem. Chem. Phys.*, 2015, **17**, 24978–24987.
15 D. W. deQuilettes, W. Zhang, V. M. Burlakov, D. J. Graham, T. Leijtens, A. Osherov, V. Bulović, H. J. Snaith, D. S. Ginger and S. D. Stranks, *Nat. Commun.*, 2016, **7**, 11683.
16 X. Fu, D. A. Jacobs, F. J. Beck, T. Duong, H. Shen, K. R. Catchpole and T. P. White, *Phys. Chem. Chem. Phys.*, 2016, **18**, 22557–22564.
17 D. Liu and T. L. Kelly, *Nat. Photonics*, 2014, **8**, 133–138.
18 N. Aristidou, C. Eames, I. Sanchez-Molina, X. Bu, J. Kosco, M. S. Islam and S. A. Haque, *Nat. Commun.*, 2017, **8**, 15218.
19 C. C. Boyd, R. Cheacharoen, T. Leijtens and M. D. McGehee, *Chem. Rev.*, 2019, **119**, 3418–3451.
20 S. P. Dunfield, L. Bliss, F. Zhang, J. M. Luther, K. Zhu, M. F. A. M. van Hest, M. O. Reese and J. J. Berry, *Adv. Energy Mater.*, 2020, **10**, 1904054.
21 K. Kwak, E. Lim, N. Ahn, J. Heo, K. Bang, S. K. Kim and M. Choi, *Nanoscale*, 2019, **11**, 11369–11378.
22 J. Even, L. Pedesseau and C. Katan, *J. Phys. Chem. C*, 2014, **118**, 11566–11572.
23 X. Wen, Y. Feng, S. Huang, F. Huang, Y.-B. Cheng, M. Green and A. Ho-Baillie, *J. Mater. Chem. C*, 2016, **4**, 793–800.
24 M. Shirayama, H. Kadowaki, T. Miyadera, T. Sugita, M. Tamakoshi, M. Kato, T. Fujiseki, D. Murata, S. Hara, T. N. Murakami, S. Fujimoto, M. Chikamatsu and H. Fujiwara, *Phys. Rev. Appl.*, 2016, **5**, 014012.
25 S. D. Stranks, V. M. Burlakov, T. Leijtens, J. M. Ball, A. Goriely and H. J. Snaith, *Phys. Rev. Appl.*, 2014, **2**, 034007.
26 M. Saba, M. Cadelano, D. Marongiu, F. Chen, V. Sarritzu, N. Sestu, C. Figus, M. Aresti, R. Piras, A. G. Lemann, C. Cannas, A. Musinu, F. Quochi, A. Mura and G. Bongiovanni, *Nat. Commun.*, 2014, **5**, 5049.
27 M. Anaya, J. F. Galisteo-López, M. E. Calvo, J. P. Espinós and H. Míguez, *J. Phys. Chem. Lett.*, 2018, **9**, 3891–3896.
28 G.-J. A. H. Wetzelaer, M. Scheepers, A. M. Sempere, C. Momblona, J. Ávila and H. J. Bolink, *Adv. Mater.*, 2015, **27**, 1837–1841.
29 H. Cao, J. Li, Z. Dong, J. Su, J. Chang, Q. Zhao, Z. Li, L. Yang and S. Yin, *ACS Energy Lett.*, 2019, **4**, 2821–2829.
30 E. Mosconi, D. Meggiolaro, H. J. Snaith, S. D. Stranks and F. De Angelis, *Energy Environ. Sci.*, 2016, **9**, 3180–3187.